energy&fuels

pubs.acs.org/EF Article

Intrinsic Solid-State Reaction Characteristics of Coals and Chars in a Direct Carbon Fuel Cell: With Focus on Significance Assessment of Fuel-Borne Factors

Chengguo Li, Hakgyu Yi, Seongyong Eom, Gyungmin Choi, Tae-Youl Choi, and Donggeun Lee*

Cite This: *Energy Fuels* 2020, 34, 4129–4138 Read Online

ACCESS | Metrics & More | Article Recommendations | Supporting Information

ABSTRACT: In this study, we attempted to evaluate relative significance of the factors that have been proposed to affect the electrochemical reaction of coals in a direct carbon fuel cell (DCFC). In the present DCFC system, we used three raw coals (bituminous, intermediate bituminous, and sub-bituminous) and the corresponding chars that were adsorbed on a porous Ni plate. The plate was then rolled to make a cylindrical anode. The intrinsic properties (e.g., gas composition, surface area, oxygen-functional groups, and nature of mineral matter in their ashes) of fuels were characterized. The electric current and potential were measured at 600 °C for anodes fueled by an equal mass (1 g) of raw coal or char. It was found that the electrochemical performance of raw coal was not sensitive to the gases evolved by the coal unless a large amount of coal was used. A striking difference in potential−current curves was observed between chars; the electrochemical activity of sub-bituminous char was much higher than that of the other chars. This was caused mainly by the larger amount of catalytic (Ca and Fe) components exposed on the surface of the char. The surface area did not have a significant effect because of its non-wetting nature.

1. INTRODUCTION

Coal is the most abundant energy resource in the world and has been mostly used in coal-fired power plants.[1] Although the most economical way to use coal has been to burn it, we now face a great challenge: minimizing emissions of greenhouse gases and ultrafine dusts from power plants while retaining the benefits of the method. The key is discovering how to use coal in a way that is both more efficient and more environmentally friendly. A direct coal fuel cell (DCFC) may be the most likely candidate. A DCFC converts the chemical energy of coals into electricity through an electrochemical reaction, which eliminates Carnot cycle constraints and offers a thermodynamic efficiency near 100%.[2−9] Additional advantages of DCFC include the fact that CO_2 does not need to be separated from flue gas, which significantly reduces expenses related to carbon capture and sequestration (CCS).

In fact, the great potential of DCFC in energy and environment applications has triggered a large number of studies over 2 decades.[10] More than 100 research articles have introduced a diversity of efforts to develop their own structures of DCFCs or to test various materials for the key system components (such as anode, cathode, and electrolyte) and fuels, in attempts to promote the system performance. It is also worth mentioning that there was a limited success in recent trials for solving the practical challenges, such as poor utilization of solid fuels[11−13] and inferior long-term operation.[14] According to Jiang et al.,[11] promoting the carbon conversion of low-grade fuels into CO at 750 °C led to increasing the maximum power density up to ∼900 mW cm^{-2}, which is comparable to conventional hydrogen-fueled fuel cells. Nevertheless, particular attention is given to the materials with focus on anode catalysts for the electrochemical oxidation of carbon and carbon fuels.[10]

As for the carbon fuels, almost any type of carbon source, starting from amorphous carbon black or graphite to more practical fuels, such as coals, biomass, and industrial wastes, can be used as a fuel for DCFCs, which makes DCFCs cost-effective. Among these fuels, carbon black and graphite have been widely used as a standard carbon fuel for a parametric study in DCFCs, because they have relatively simple properties. In this study, however, we selected coals on account of their practical importance in the real world, such as abundance of natural reserves, high cost competitiveness, and environmental impact.

One problem is that the electrochemical reactivity of coals is not stable but heavily dependent upon intrinsic properties, such as the reactant volatile species (H_2, CH_4, and CO) evolving from the coals, the contents of carbon-containing functional groups, and the specific surface area and catalytic ash components (Ca, Fe, Mg, etc.) of the coals.[8−19] In fact, it is not scarce to find conflicting results in previous studies for using coals and chars in DCFCs. The following are several examples: Ahn et al.[16,17] evaluated the electrochemical characteristics of coals, biomass char, and industrial waste in a molten carbonate (MC)-based DCFC system. They investigated the effect of the specific surface area on the

Received: December 18, 2019
Revised: March 2, 2020
Published: March 3, 2020

https://dx.doi.org/10.1021/acs.energyfuels.9b04387
Energy Fuels 2020, 34, 4129−4138

Table 1. Proximate and Ultimate Analyses of Feedstocks

	proximate analysis (wt %, air dried)				ultimate analysis (wt %, air dried)				
fuel	moisture	volatile matter	fixed carbon	ash	C	H	O	N	S
coal A	2.54	32.94	46.60	17.92	69.20	4.03	6.78	1.72	0.77
coal B	13.86	41.65	38.75	5.75	77.50	4.85	8.90	1.67	1.56
coal C	17.53	38.78	38.13	5.56	58.95	5.38	14.29	0.66	1.32
char A	3.05	3.71	69.07	24.18	69.10	0.75	8.24	0.68	1.18
char B	4.30	7.83	77.05	10.83	80.97	1.23	7.48	0.60	1.81
char C	6.37	8.80	77.36	7.47	84.82	0.95	5.24	0.84	1.65

electrochemical performance of samples.[16] In another study,[17] they claimed that the electrochemical performance of the samples is mainly determined by the content of the carbon-containing functional groups. Eom et al. used a similar MC DCFC system to examine the electrochemical performance of coals and reported that the power density of the coal increased with increasing volatile species content.[18,19] Li et al.[8] argued that the aforementioned fuel-borne factors may all contribute to enhancing the electrochemical reactivity of the coals.

As such, these seem to manifest that the research community has not yet reached a solid consensus even on the basic question, i.e., what the most fundamental fuel-borne factor is. The main reason might be associated with the difficulty in isolating the fuel-borne factors as well as the diversity of coal types and properties. When it comes to the acid or base pretreatment of coals that has recently been proposed,[10] it will inevitably result in simultaneous changes of surface area, pore volume, surface functional groups, and catalytic ash contents of coals. Similarly, either the use of coal gasification or high-temperature operation of the DCFC cell[10,11] might be a practical method for easy fuel supply with higher reactivity[13,14] but not appropriate for a parametric study.

Here, we would like to recall that the benefit of DCFCs (the highest thermal efficiency) is attainable only through the direct reaction of solid carbon.[2] It sounds simple, but there is a practical challenge arising from the Boudouard reaction ($C + CO_2 = CO$)[20−22] and/or gasification of coals into gaseous fuels, such as H_2, CO, and CH_4.[11,17,18] Once the gaseous fuels (often called syngas) that are more reactive than solid carbon are produced in an anode of the DCFC cell, the cell performance will be determined mainly by the gaseous fuels. Under these circumstances, it becomes impossible to clarify the intrinsic solid-state reactivity of the coals. This would be aggravated if coals with a high content of volatile matter are tested at high temperatures.

Taking this into account, we would propose two methods for identifying the intrinsic reactivity of coals and chars: lowering the amount of coal samples to minimize the coal gasification and operating the DCFC system at 600 °C to deactivate the Boudouard reaction. Meanwhile, another concern may arise from the low-temperature operation of DCFCs because it has often resulted in unacceptably low power generations.[23,24] Hence, another mission of our study is to demonstrate that our DCFC system is operating with an acceptable performance at that temperature.

For these multipurposes, we prepared and used three different raw coals (and their corresponding chars) as fuel for our unique MC-based DCFC system.[13,14] Each fuel was characterized in terms of volatile species, surface functional groups, specific surface area, ash components, and resulting syngas compositions. As mentioned before, a small amount of fuel (1.0 g for each of coals or chars) was applied and tested at a low operation temperature of 600 °C. Upon increasing the fuel mass, the syngas compositions were monitored and compared to changes in electrochemical reaction characteristics. In connection with the fuel properties, the fuels were carefully treated or additionally selected to isolate each fuel-borne factor, such as volatile species, surface area, and ash components. As a result, the effects of fuel properties on the intrinsic electrochemical reactivity could be almost independently evaluated. Lastly, a porous Ni anode was employed to enhance fuel−anode contact and to increase the maximum power density to an acceptable level, even at 600 °C.

2. EXPERIMENTAL SECTION

2.1. Fuel Preparation. Three different grades of raw coal provided by a Korean coal-fired power plant were prepared to facilitate a comparison of fuel characteristics and electrochemical reactivity. Coal A (named Moolarben) and coal C (Berau) were bituminous and sub-bituminous coals, respectively, while coal B (Indominco) was classified as an intermediate coal, whose properties are somewhat closer to the sub-bituminous coal. All samples were sieved to 75−150 μm size and dried at room temperature for 1 day prior to experimentation. Any remaining moisture was then removed from the raw coals by heating them at 120 °C for 1 h. The chars were prepared using a raw coal carbonization process, by heating the coals from 25 to 900 °C at a rate of 10 °C min^{-1} under Ar flow.

The composition of the fuel samples was characterized using the proximate and ultimate analyses and is summarized in Table 1. For the proximate analysis, a thermogravimetric analysis (TGA, SDT-Q600, TA Instruments) was conducted in accordance with ASTM E1131. The ultimate analysis was performed using a vario MICRO cube, which was subjected to a temperature of 1150 °C, with sulfanilic acid used for the standard solution.

2.2. Analytical Characterization of the Physicochemical Properties of the Fuels. Various analytical techniques were employed to analyze the physicochemical properties of raw coals and chars in a DCFC system. The thermal properties of the fuels (with a focus on their volatility) were investigated using TGA (Q-50, TA Instruments, New Castle, DE, U.S.A.) under an Ar flow of 100 mL min^{-1}. After the fuels were heated from room temperature to 900 °C at a heating rate of 10 °C min^{-1}, the volatile gas species evolved from the fuels were analyzed for CH_4, H_2, and CO by gas chromatography (GC, 8610C, SRI Instrument).

Two techniques were employed to investigate the specific surface areas, pore volumes, and surface functional groups of the fuels. The nitrogen gas adsorption characteristics of the fuels were investigated using a Micromeritics surface area analyzer (ASAP 2020, Micromeritics Co., Norcross, GA, U.S.A.). The Brunauer−Emmett−Teller (BET) analysis was then applied to obtain the surface area and pore volume. Additionally, gas adsorption and desorption tests were conducted for two ranges of relative pressures, P/P_0 = 0.05−0.95 and 0.95−0.1, respectively. The pore diameter (D_{pore}) of the fuels was determined using the Barrett−Joyner−Halenda (BJH) method.[16−19]

The elemental surface composition of the raw coals and chars was measured by X-ray photoelectron spectroscopy (XPS, Theta Probe angle-resolved X-ray photoelectron spectrometer (ARXPS), Thermo

https://dx.doi.org/10.1021/acs.energyfuels.9b04387
Energy Fuels 2020, 34, 4129−4138

Fisher Scientific). The incident radiation that was used was a monochromatic Al Kα line (1486.6 eV) with 150 W (15 kV and 10 mA). Survey scans were taken for a range of binding energies (0–1000 eV) with a resolution of 1.0 eV.

2.3. DCFC System. Figure 1 shows a schematic diagram illustrating the preparation of the anode used in this study. A 6 cm long, 3 cm wide porous Ni plate (with a pore size of 50–150 μm) was used as the base-supporting structure of the anode. A constant amount of fuel for each of the three types of raw coals and chars was spread on the surface of the Ni plate; 1 g of fuel was used, unless otherwise noted. The Ni plate was then rolled to hold the fuels in the form of a cylinder (3 cm long and 1 cm diameter), aiming at enhancing contact (active sites) between the anode and fuel particles.

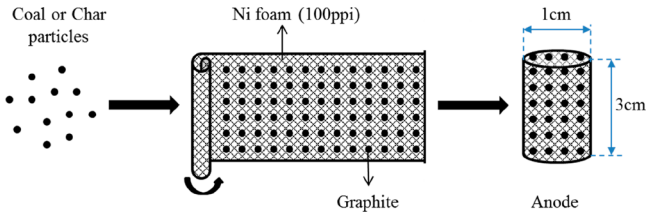

Figure 1. Schematic diagram for manufacturing a tubular anode; the fuel sample was placed on the surface of a porous Ni anode, and the anode was then rolled into a cylinder.

The electrochemical oxidation characteristics of the fuel-filled porous Ni anode were measured in a three-electrode electrochemical cell,[13,14] as shown in Figure 2. The cylindrical Ni anode containing the fuel was used as a working electrode (WE), after being spot-welded to a flat plate-type silver current collector (6 cm high × 0.4 cm wide). The counter electrode (CE) and reference electrode (RE) were made from a silver sheet (3.2 cm^2 surface area) that was spot-welded to a silver wire; the silver parts were sheathed in a 12 mm diameter closed-bottom alumina tube. A 1.0 mm hole at the bottom of the alumina sheath allowed for the conduction of carbonate ions between the electrodes through a MC electrolyte. The electrolyte, a 350 g mixture of Li_2CO_3 and K_2CO_3 with a molar ratio of 62:38, was placed in an alumina container and melted at 600 °C. Thus, when the carbon-containing WE was immersed in the MC-containing alumina container, the WE was wetted in contact with the MC, resulting in a significant enhancement of the triple-phase boundary (TPB).

Prior to measuring the electrochemical performance of the system, any residual oxygen was removed during the warming process of the system by flowing CO_2 gas into the CE and RE at a rate of 50 mL min^{-1}. When the 600 °C operating temperature was reached, a mixture of CO_2 and O_2 (with a mole ratio of 2:1) was injected into the CE and RE at an overall flow rate of 100 mL min^{-1}. During the electrochemical reaction of carbon, Ar gas was continually supplied to the WE at 200 mL min^{-1}, to purge any CO_2 gas that had been produced.

The electric current and potential of the DCFC system were then measured using a SP-150 potentiostat/galvanostat analyzer (Neoscience, Korea) with a scan rate of 1 mV s^{-1}. The measured electrical potential (V) was the voltage difference observed between the WE and RE, while the current was being monitored from the WE to the CE. Because the RE was in proximity to the WE and was electrically separated from the CE, the electric potential of the WE (versus RE) could be regarded as an anode potential. Under open circuit conditions, the electric potential (versus RE) could correspond to the open circuit voltage (OCV) and the potential of RE was confirmed to be very close to that of the CE. Note that the electric current density (I) was obtained by dividing the measured current by the apparent contact area between the fuel particles and the Ni plate (18 cm^2, measured before rolling) (see Figure 1). Given a current density and an anode potential, the power density (P) was simply calculated by multiplying the values of I and V. To better understand the I–V characteristics, electrochemical impedance spectroscopy (EIS) was measured using the SP-150 analyzer at a frequency range from 0.2 Hz to 40 kHz. Further details about the instrumentation and measurements are available elsewhere.[12–14]

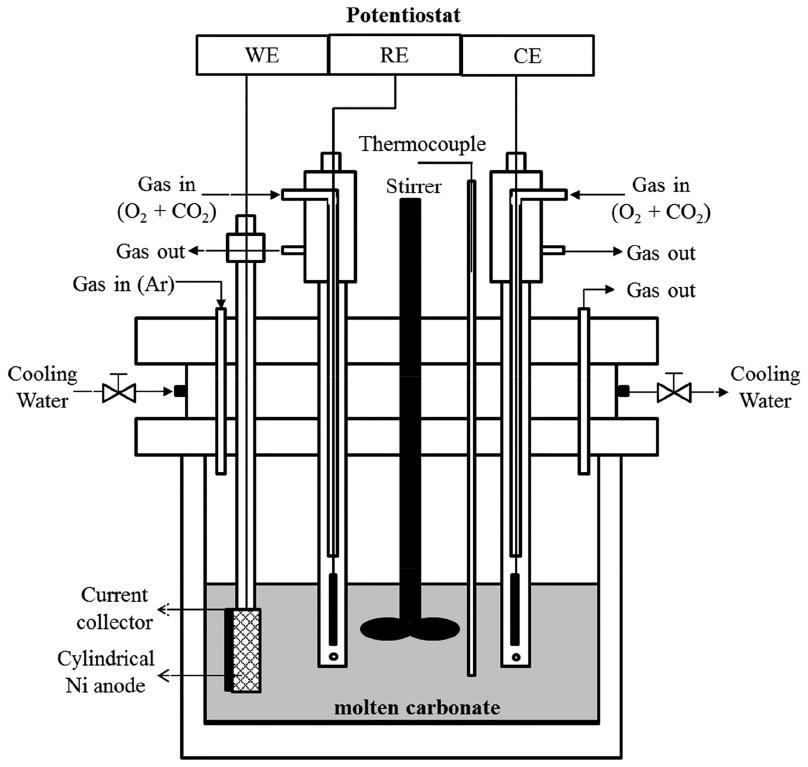

Figure 2. Schematic diagram of a three-electrode DCFC measurement system.

https://dx.doi.org/10.1021/acs.energyfuels.9b04387
Energy Fuels 2020, 34, 4129–4138

3. RESULTS AND DISCUSSION

3.1. Characterization of Physicochemical Properties of the Fuels. Figure 3 shows the TGA profiles of the fuel samples (i.e., raw coals and chars) measured in an Ar atmosphere. It can be said that most of the volatile matter in the raw coals is removed by the char-making process (i.e., heating the coals from 25 to 900 °C at a rate of 10 °C min^{-1} under Ar flow). The TGA data for the raw coals indicate that a substantial amount of volatile matter is released at temperatures of 300−500 °C by thermal decomposition and/or evaporation.[18,20,25] Above 600 °C, however, the raw coals only exhibit a 3−7% decrease in mass; this suggests that, at such high temperatures, the raw coals are close to the chars in nature and their surfaces might be dominated by non-volatile species, such as carbon or ash. On the other hand, the masses of char A, B, and C decrease only slightly, to a maximum of 6% across all temperatures. This implies that the chars exist primarily in a solid phase and that they contain a negligible amount of volatile matter, regardless of the fuel type.

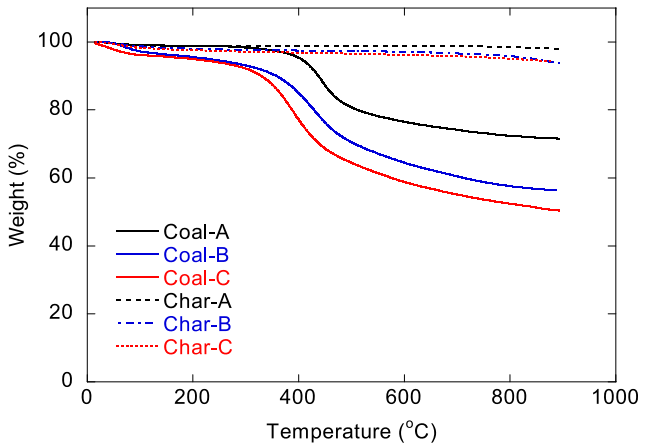

Figure 3. Thermal reactivity of samples in TGA under an Ar atmosphere.

The specific surface area, pore volume, and average diameter of pores obtained by the BET method are presented in Table 2. The specific surface areas of the three types of raw coals are all similar (approximately 3 m^2 g^{-1}), suggesting that the raw coals are almost non-porous. However, the corresponding chars have significantly different pore characteristics: the char from the sub-bituminous coal (char C) is highly porous, with the largest specific surface area observed in the study (217 m^2 g^{-1}), while the char from the bituminous coal (char A) is least porous. It is interesting to note that the pore size is not significantly different between the chars. With respect to the anodic reaction ($C + 2CO_3^{2-} \rightarrow 3CO_2 + 4e^-$), one may speculate that the most porous char C would be the most reactive in the case where the surface pores of the chars could be accessed by carbonate ions.[16−19]

Table 2. BET Results of Raw Coals and Chars

	N_2 adsorption (77 K)		
fuel	S_{BET} (m^2 g^{-1})	V_{total} (cm^3 g^{-1})	D_{pore} (nm)
coal A	3.33	0.0054	11.49
coal B	3.82	0.0015	1.22
coal C	3.32	0.0013	1.66
char A	72.25	0.025	2.14
char B	126.78	0.062	1.96
char C	217.55	0.112	1.92

The functional groups on the surface of the raw coals, such as volatile hydrocarbons, or oxygenated surface groups, including carbonyl, carboxyl, and hydroxyl groups,[26] could be transformed into gaseous hydrocarbons and CO at high temperatures. Both of these gases can react electrochemically with carbonate ions. Consistent with previous studies,[8,16−19] we used XPS to measure the O/C ratios indicative of the surface functional groups. The XPS results are summarized in Table 3. In the case of raw coals, the highest and lowest carbon contents are observed in coals B and C, respectively. These results are reversed for the O content, which is lowest in coal B and highest in coal C. Because coal C shows the highest O/C ratio (that is, it is the most oxygenated), it might be the most reactive.[16,18] It is, however, noted that the char samples have similar O/C ratios (~20%), regardless of their pristine coal types.

The mineral impurities on the surface of the fuels are also analyzed by XPS. Table 3 shows that the relative catalytic species contents (Ca and Fe[8]) of the chars are all significantly larger than those of the raw coals. This suggests that volatile organic matter and surface oxygenated groups are removed to expose the catalytic species (mainly in the form of oxides) during the char-making process. Among the chars, the char C sample has the most catalytic species on its surface. According to Castellano et al.,[27] such surface oxides could act as mediating sites for the exchange of O^{2-} ions, facilitating the adsorption of O^{2-} to the electrode surface and the subsequent anodic reaction with neighboring carbon particles. In contrast, Si and Al oxide species, particularly if they exist on a surface, could be dissolved to form passive layers at the electrode surface and could thus deactivate some local part of the electrode.[28] In this respect, Table 3 indicates that the raw coals seem to be less reactive than their chars, having lower surface passivating contents and higher surface catalytic contents.

3.2. Electrochemical Reaction Characteristics of Raw Coals and Chars. Figure 4 shows the $I-V-P$ characteristics of the three types of raw coals and chars under the same experimental conditions (at 600 °C). In Figure 4a, coals B and C show similar $I-V$ curves, while coal A has a slightly lower power density. Here, all of the raw coals have similar fixed carbon contents and specific surface areas, as shown in Tables 1 and 2, while surface oxygenated groups (in terms of the O/C ratio) and volatile matters are substantially lower for coal A relative to the other raw coals (see Tables 1 and 3). Indeed, both volatile matter and surface oxygenated groups can produce gaseous CO and H_2 fuels at low temperatures of 300−500 °C. Because gaseous reactants, such as CO and H_2, are known to be more electrochemically reactive than solid carbon,[18,29] the lower reactivity of coal A might be attributed to its lower volatility (i.e., its capacity to emit reactive gases).

To verify this conjecture, the composition of gas evolving from the raw coals was analyzed with GC. For the GC measurements, 1 g of each sample was heated from room temperature to 600 °C at a rate of 5 °C min^{-1}. The temperature was then held constant for 2 h. This heating process is similar to the warming process used in the present DCFC operation. Panels a, b, and c of Figure 5 show the transient emissions of H_2, CH_4, and CO from the three raw coals, respectively. As expected, coal A is the least volatile, emitting few gases. In contrast, coals B and C are clearly more

https://dx.doi.org/10.1021/acs.energyfuels.9b04387
Energy Fuels 2020, 34, 4129−4138

Table 3. XPS Results of Raw Coals and Chars

fuel	C 1s (wt %)	O 1s (wt %)	N 1s (wt %)	Si 2p + Al 2p (wt %)	Ca 2p + Fe $2p_{3/2}$ (wt %)	O/C (%)	N/C (%)	(Si + Al)/C (%)	AI (%)
coal A	65.22	21.14	2.91	8.28	0.14	32.04	4.41	12.52	
coal B	55.64	20.35	5.52	10.62	0.84	36.52	9.88	19.01	
coal C	44.38	34.34	1.17	15.11	0.88	77.48	2.45	34.05	
char A	74.51	15.69	1.38	6.23	0.47	20.99	1.73	8.36	8.1
char B	64.08	17.68		6.24	2.54	27.58		9.68	40.9
char C	68.79	13.78	2.49	7.78	5.24	20.01	3.42	11.21	67.0

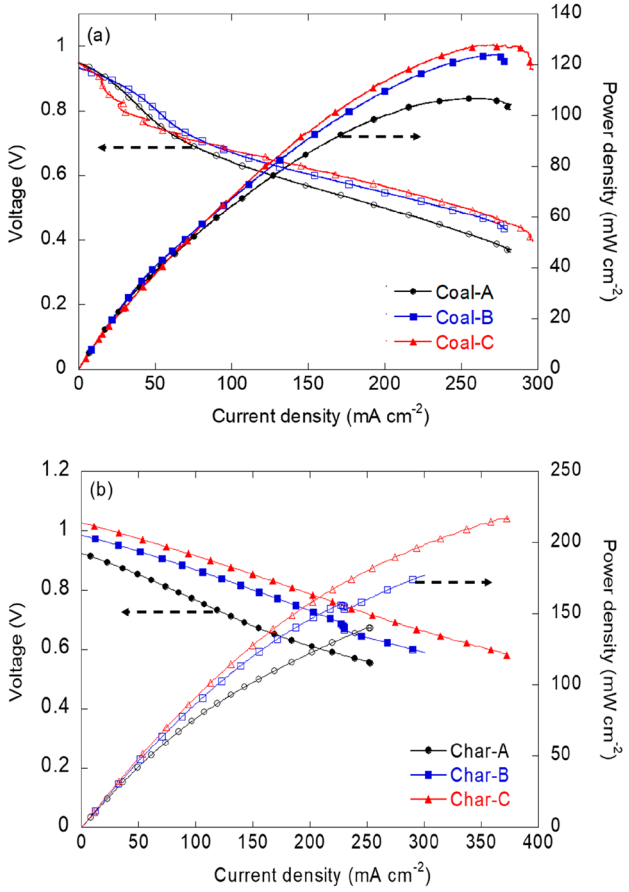

Figure 4. Potential (V) and power density profiles versus current density (I) for each (a) raw coal and (b) char at 600 °C.

volatile, emitting a similar level of CO at a time of approximately 100 min from the beginning of the heating. CH_4 emissions are only detected from coal C.

Doubtlessly, the evolving CO and H_2 gases can be used as additional fuels to produce electrons, like they are used in MCFCs via $CO + CO_3^{2-} \rightarrow 2CO_2 + 2e^-$ and $H_2 + CO_3^{2-} \rightarrow CO_2 + H_2O + 2e^-$.[18,29] In contrast, CH_4 probably does not take a direct electrochemical route in the present MC-based environment (unlike in solid oxide fuel cells).[30,31] Instead, CH_4 is preferentially cracked into C and H_2 to participate in anodic reactions of C and H_2. Because the thermal CH_4 cracking is thermodynamically limited below 700 °C,[13] CO produced from coals B and C (in Figure 5c) seems to make a positive contribution to increasing the power density of the fuels relative to coal A.

To investigate the role of the gases further, the gas analysis and $I-V$ measurement was repeated with increased fuel masses of 5 and 10 g. These experiments were considered only for coal C, because coal C has the largest amount of volatile species.

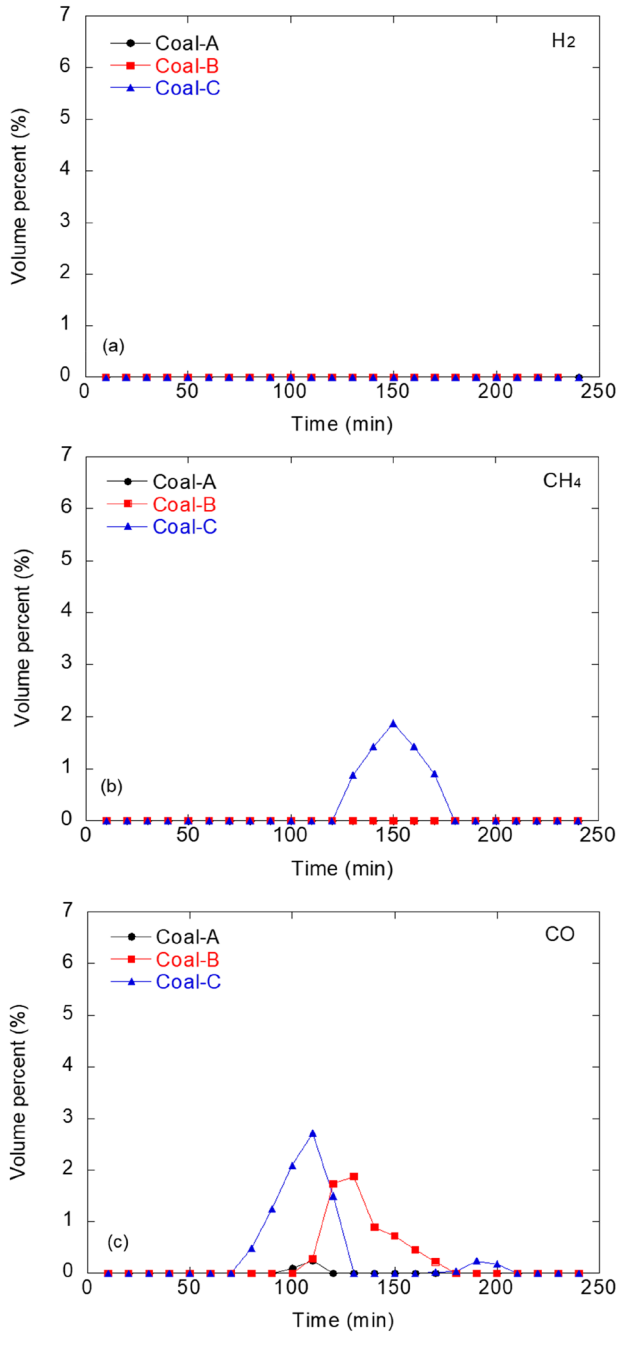

Figure 5. Volume percent of produced gases, such as H_2, CH_4, and CO, from raw coal samples of 1 g at 600 °C.

Panels a–c of Figure 6 show the transient evolution profiles of H_2, CH_4, and CO from different masses of coal C. Overall, more gases are produced upon increasing coal mass. The most

https://dx.doi.org/10.1021/acs.energyfuels.9b04387
Energy Fuels 2020, 34, 4129–4138

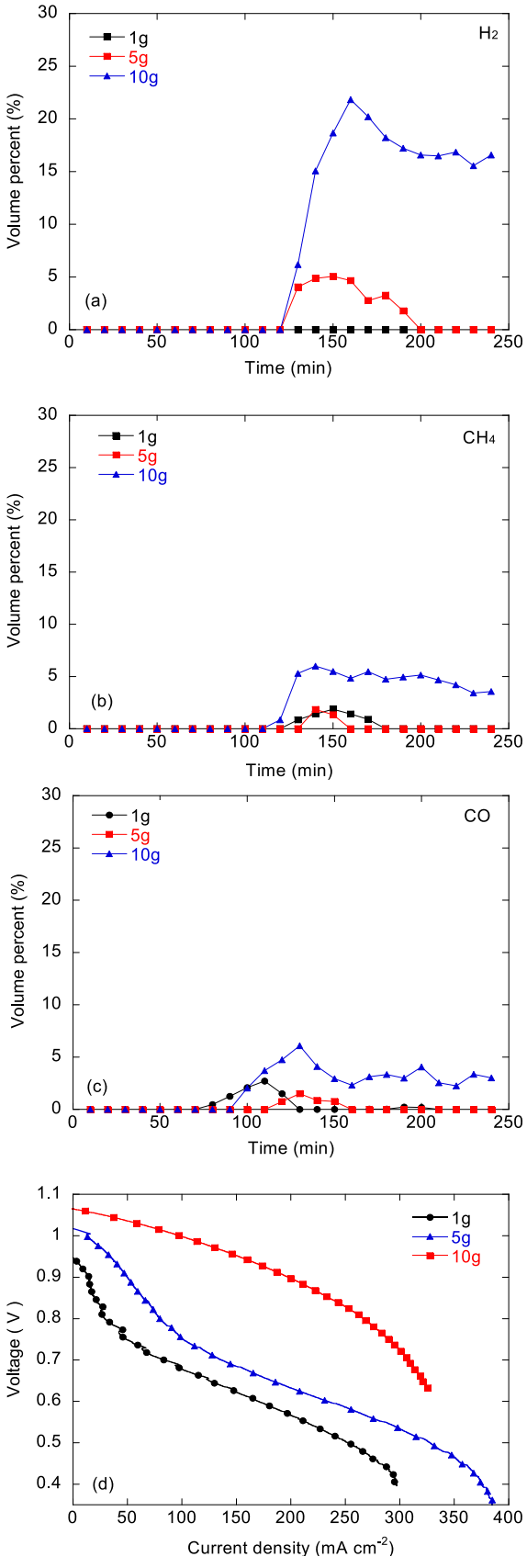

Figure 6. Volume percent of produced gases with three different masses (1, 5, and 10 g) of coal C: (a) H_2, (b) CH_4, and (c) CO and (d) corresponding potential−current density curves.

dramatic change is observed for H_2, as seen in Figure 6a; its concentration increases from 0 to 20 vol % when increasing the coal mass by a factor of 10. In addition, the coal could produce CH_4 and CO at values as high as 10 and 8 vol %, respectively. It is also noted that the coal gasification is continued for longer than 4 h after the start of heating.

Figure 6d shows that the $I-V$ characteristics for coal C are highly dependent upon the coal mass. Upon increasing the coal mass, the OCV steadily increases up to 1.06 V, beyond the ideal value (1.02 V) of carbon,[4] indicating the potential contribution of gaseous fuels[32] (OCV for H_2 is 1.065 V, and OCV for CO is 0.897 V). Up to 5 g, the coal exhibits similar $I-V$ characteristics, characterized by a large activation overpotential: a rapid potential decrease from OCV to ∼0.75 V is observed in low current regions ($I < 100$ mA cm^{-2}). This is a typical sign of a large activation resistance for a solid carbon in a DCFC. However, when the fuel mass increases to 10 g, the results show a typical $I-V$ curve shape for gaseous fuels, denoting negligible activation resistance, as is typical of a MCFC at high temperatures. This finding suggests that the gases that evolve from coal, which are more reactive than the coal itself, can dominate the anodic reaction in a DCFC, particularly when a large amount of solid fuel is used. Under these circumstances, it is very difficult to measure the intrinsic reactivity of the solid coal or the individual impacts of fuel-borne properties. This justifies why the fuel mass was minimized to 1 g in this study and explains why the influence of coal volatility on power density was fairly low, as shown in Figure 4a.

3.3. Effects of the Specific Surface Area and Catalytic Components in the Chars. Now let us return to Figure 4, recalling that the purpose of this study is to assess the intrinsic effects of various fuel-borne factors on DCFC performance. Figure 4b shows $I-V-P$ curves for the chars prepared from the three types of raw coals. In comparison to the raw coals in Figure 4a, the chars show relatively strong coal-type dependency in their power density: the maximum power densities are found to be 140, 180, and 230 mW cm^{-2} for chars A, B, and C, respectively. Among the factors, the fixed carbon content and surface oxygen groups given by the O/C ratio are not significantly different between the chars (see Tables 1 and 3), and thus, these factors are ruled out.

However, as indicated in Tables 2 and 3, the specific surface area (S_{BET}) and the contents of Ca and Fe on the char surface are very different between the chars. Let us first address the surface components. Because the Ca and Fe components existing in the form of oxides are known to accelerate the anodic reaction of carbon as catalysts, they are categorized as activating species. In contrast, the components of Si and Al, coming from SiO_2 and Al_2O_3 in surface ash, are known to hinder the anodic reaction and are known as deactivating species.[28,33−35] Hence, the relative activity of the surface ashes is assessed with an alkaline index (AI) of ashes, which is defined by the content of the activating (catalytic) species relative to the deactivating species. The AI values of the three chars were calculated on the basis of the XPS data and listed in Table 3. Char C shows the highest AI value (67%); char B has the second highest AI value at 40.9%; and char A has the least active ash, with an AI value of 8.1%. In summary, the three chars range in order of AI as char C > char B > char A, which is interestingly in agreement with the order of the char's power densities.

https://dx.doi.org/10.1021/acs.energyfuels.9b04387
Energy Fuels 2020, 34, 4129−4138

Table 4. Ash Constituent Analysis (wt %) of Raw Coals

	SiO_2	Al_2O_3	CaO	Fe_2O_3	TiO_2	K_2O	MgO	Na_2O	P_2O_5
coal A	81.4	11.8	1.7	1.4	0.9	0.5	0.5	0.4	0.3
coal B	46.3	18.5	10.1	8.3	0.8	1.7	4.2	3.1	0.3
coal C	31.6	14.9	16.7	10.3	0.8	0.7	4.5	2.7	0.6

Table 5. Comparative Properties of Chars C and D

XPS measurement							
fuel	C 1s (wt %)	O 1s (wt %)	Si 2p + Al 2p (wt %)	O/C (%)	CaO (%)	Fe_2O_3 (%)	AI (%)
char C	68.7	13.7	7.7	20.0	4.4	0.7	67
char D	71.9	18.2	9.1	25.3	0.8	0.1	9.9
proximate analysis (wt %, air dried)							
	moisture	volatile matter	fixed carbon	ash			
char C	6.3	8.8	77.3	7.4			
char D	8.9	7.8	78.8	10.8			
BET: N_2 adsorption (77 K)							
	S_{BET} (m^2 g^{-1})	V_{total} (cm^3 g^{-1})	D_{pore} (nm)				
char C	217.55	0.11	1.92				
char D	212.29	0.12	2.71				

Besides the catalytic components on the char surface, the entire composition of the ash might also be important, because carbons on the char are continually consumed during DCFC operation, which gradually exposes internal layers of the char to incoming carbonate ions. Thus, the ashes that remained after the raw coal was burned were chemically analyzed with X-ray fluorescence (XRF-1700, Shimadzu, Japan). Table 4 summarizes the measured weight percentages of the oxide species in the ash. All coal ashes are dominated by SiO_2, with significant inclusions of Al_2O_3, CaO, Fe_2O_3, and MgO. Other constituents are minor, at less than 2 wt % of the total ash. Char C is distinct from the other samples; among the chars, it has the lowest content of deactivating species and the highest content of catalytic species. Char A is opposite in composition to char C. These results are qualitatively consistent with the XPS results.

There is another factor, S_{BET} of the chars shown in Table 2, which is also well-correlated with power density. Thus, the significance of catalytic ash components relative to surface area must still be discriminated. For this purpose, we tested several sub-bituminous coals used in coal-fired power plants in Korea and selected a coal (named Adaro) with very similar char properties to char C. The char prepared from this additional coal was named char D and was subjected to proximate analysis, XPS measurement, and BET experiments. In Table 5, the results for char D are summarized in comparison to those for char C. Both of the chars have fairly similar properties, such as fixed carbon and ash contents, specific surface area, volatility, and O/C ratio. The only remarkable difference is that char D has 5 times less catalytic species than char C; the AI of char D is only 9.8%.

Figure 7 compares the $I-V-P$ characteristics of chars C and D. Char D exhibits considerably lower power density than char C. The difference in power density seems to come from the catalytic components. It should also be noted that char D has a comparable power density to char A, even though char D has a much larger specific surface area (see Tables 2 and 5). Recalling that chars D and A have similar AI values, one might conclude that the surface areas of the chars have no effect on electrochemical performance, at least under the conditions

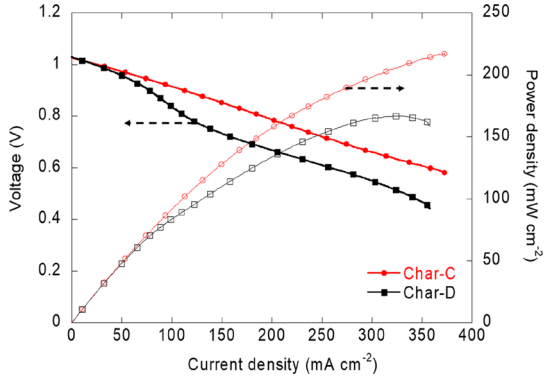

Figure 7. Potential (V) and power density profiles versus current density (I) for chars C and D at 600 °C.

used in this study. To reconfirm this, the S_{BET} and AI values of the four chars are plotted against their corresponding power densities in panels a and b of Figure 8. As expected, power density is closely correlated only with AI.

Here, it is interesting to see if the catalytic effect of ash components will be reproduced with a powder mixture of carbon and one of the catalytic species. For this purpose, a commercial powder of pure graphite was well-mixed with one of three commercial powders of CaO (30 nm, purity of 99.9%), Fe_2O_3 (50 nm, purity of 99.99%), and SiO_2 (10−20 nm, purity of 99.9%) from Aldrich. Note that the content of each oxide component was kept constant at 13 wt %, which is similar to ash contents of chars C and D in Table 5, and thus, there is no other factor involved. A fixed amount (1 g) of the mixture samples as well as the graphite alone was tested by the same procedure as employed in Figure 4.

Figure 9 clearly shows that both CaO and Fe_2O_3 can promote the electrochemical reaction of carbon as a catalyst, while SiO_2 plays a role of deactivator as expected. Another thing to note is that the maximum current density of the 13% CaO sample is around 140 mA cm^{-2}, much lower than those of all of the char samples in Figure 4. This might be attributed to the poor contacts between carbon and oxide particles that can limit their catalytic function.

https://dx.doi.org/10.1021/acs.energyfuels.9b04387
Energy Fuels 2020, 34, 4129−4138

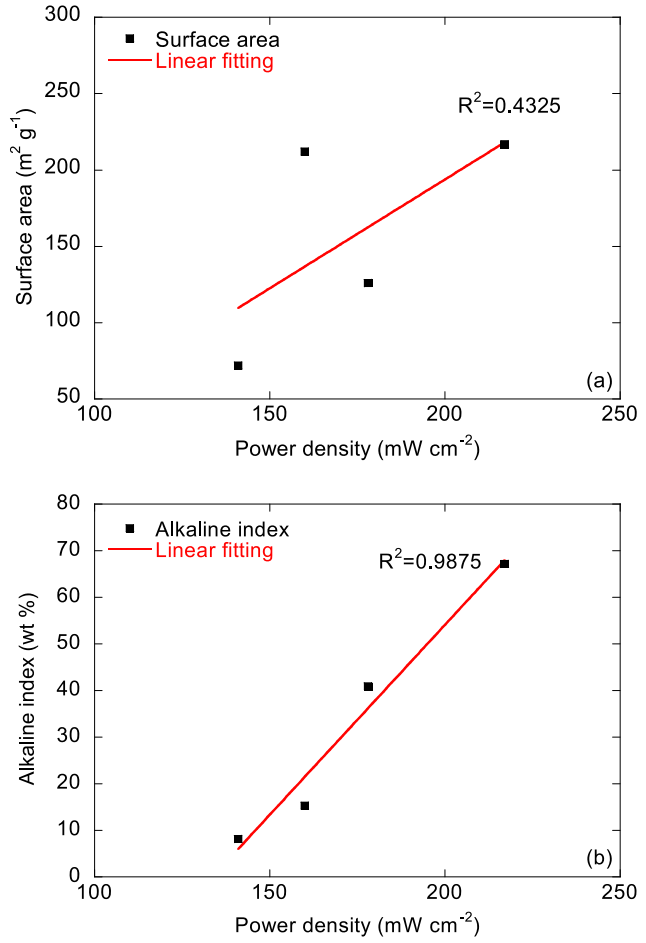

Figure 8. Relationship between P_{max} at 600 °C and (a) surface area or (b) alkaline index of chars.

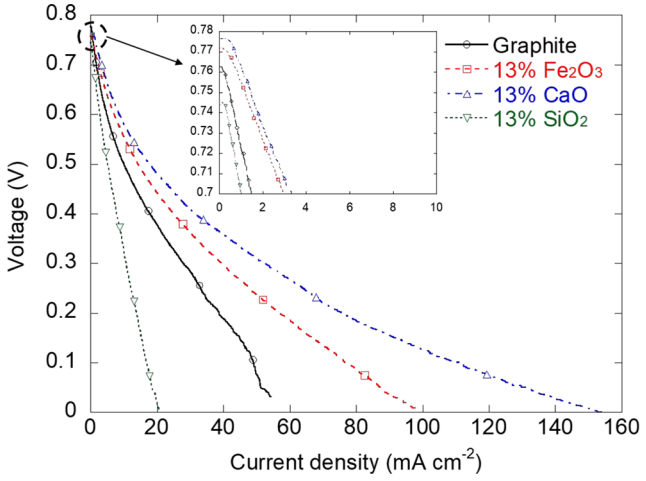

Figure 9. Potential (V) profile versus current density (I) for three different mixture samples as well as graphite alone at 600 °C.

One last question is why the surface pore structures in terms of S_{BET} do not play a significant role in the power generation particularly in the presence of strong catalysts. This might be associated with the accessibility of the surface pores to the MC liquid. The possibility of pore wetting of the MC liquid is basically not different from the well-known subject of spontaneous imbibition of liquids,[36,37] which describes the phenomenon of a wetting fluid invading a porous medium. Liquid propagation through pores occurs naturally as a result of the action of capillary forces generated within the pores. In contrast, medium pores in contact with a non-wetting liquid do not wet; they remain dry. For example, a hydrophobic microporous polyethylene membrane is not wet with water.[37]

To characterize the surface pores of the chars as wettable or non-wettable, a contact angle was measured from an image of a MC drop on a flat carbon plate. A scoop of MC powder, weighing 300 mg, was put on a flat surface of carbon and then melted at 520 °C in an Ar atmosphere. More details about this process are available in our previous work.[12] Figure S1 of the Supporting Information shows a clear image of a hemispherical MC drop resting on top of a flat plate of carbon. The contact angle was measured at 110.9°, indicative of the non-wetting nature of the char particles.

Of particular interest is to estimate the external force that is required to initiate non-wetting MC liquid flow through the pores. The pore is modeled as a cylindrical capillary tube with a fixed radius (r). On the basis of the Poiseuille flow (related to the liquid flow through a capillary), the flow velocity (V) of the liquid is frequently calculated using the Washburn equation:[38] $V = r^2/(8\mu)(\Delta P - P_c)/L$, where μ is the viscosity of the liquid, L is the length of the capillary, P_c is the capillary pressure, and ΔP is the external pressure forcing the liquid to flow.

It is obvious that $\Delta P \geq P_c$ yields a positive flow velocity of $V \geq 0$, indicating liquid penetration through the pore. Hence, P_c becomes the required minimum external pressure and is usually calculated from the measured contact angle (θ) and surface tension (γ) of the liquid by the Young−Laplace equation: $P_c = 2\gamma \cos(\theta)/r$. In the present study, the pore radius ($r \sim 1.15$ Å) is half the pore diameter of the chars in Table 5, the contact angle (θ) is 110.9°, and the surface tension (γ) is 0.2 N/m for the MC liquid.[39] Given these properties, P_c is calculated as 3.5×10^4 atm, 4 orders of magnitude larger than the operating pressure (~1 atm) of the present DCFC system. Conversely, a minimum pore diameter of 4.0 μm is required for spontaneous imbibition of the MC liquid into the carbon pores under $P_c = 1$ atm. This implies that the surface pores of the chars are too small to be accessed by the MC liquid, and thus, the surface area does not exert any significant effect on power generation.

It is worth noting that there have been conflicting claims against the surface area effect. Vutetakis et al.[4] reported that highly porous activated carbon denoted lower current density than less porous coals at 700 °C. Cooper and co-workers[40] concluded that the surface area effect of carbons alone is relatively weak. More recently, Eom et al.[41] tested three different coals as DCFC fuels at 700 °C and confirmed that there was no surface area effect. Here, it is interesting to recall the conclusion of Li et al.[8] that the microporous (<2 nm) surface of carbon is not accessible unless the surface has sufficiently large pores, which seems to be qualitatively consistent with our conclusion in this study.

On the other hand, Ahn et al.[16,17,11,12] found that the surface area of coals and biomass chars was correlated with their electrochemical power density to some degree. However, the power density was also correlated with O/C ratios and ash contents of the fuels. Cao et al.[42] reported that activated carbons, after being demineralized by various acids, become more microporous, increasing the surface area (from 958 to 1016 m^2 g^{-1}) and the current density (from 10 to 95 mA cm^{-2}). However, such a large increase in the current density is very unlikely caused by the 6% increase of the surface area.

https://dx.doi.org/10.1021/acs.energyfuels.9b04387
Energy Fuels 2020, 34, 4129−4138

Rather, the promoted reaction might be associated with changes in the surface state by the acid treatments, e.g., creation of new surface functional groups, removal of inert species in surface ash, and changes in surface acidity.[42] In addition, their DCFC operates at high temperatures of 750−850 °C, which allows other factors, such as carbon gasification, to be involved. In summary, the surface area or surface pore structure does not play any significant role at least under the process conditions of this study.

4. CONCLUSION

This study was devoted to a careful assessment of various fuel-borne factors affecting the electrochemical performance of a DCFC. The factors include temperature-dependent volatility, evolving gas composition, and surface functional groups in terms of the O/C ratio, ash content, and composition of coals. Bituminous, sub-bituminous, and intermediate coals and their corresponding chars were tested as fuels for the DCFC system. Our unique approach to the study was to use a fixed (minimum) amount of fuel and to lower the DCFC operating temperature to 600 °C. As a result, the volatile species emitted mostly H_2, CO, and CH_4, and their contribution to the cell performance could be minimized, unless a sufficiently large amount of fuel is used. After the char-making process, three types of chars showed remarkable differences in surface area and surface contents of catalytic ash components. A sub-bituminous char with the largest surface area and the highest alkaline index performed best in DCFC operations; its power density reached 230 mW cm^{-2}. When a reference char sample was tested as well, it was shown that the surface pores of the chars could not serve as extended active sites, because of their non-wetting nature. Instead, the surface catalytic components of the chars (in terms of their AI index) directly impacted electrochemical performance, at least under the conditions used in this study. This finding was further supported by the extra experiment using commercial samples.

■ ASSOCIATED CONTENT

Supporting Information

The Supporting Information is available free of charge at https://pubs.acs.org/doi/10.1021/acs.energyfuels.9b04387.

Contact angle of a hemispherical MC electrolyte on a flat graphite plate (Figure S1) (PDF)

■ AUTHOR INFORMATION

Corresponding Author

Donggeun Lee − *School of Mechanical Engineering, Pusan National University, Busan 609-735, South Korea;* orcid.org/0000-0001-7256-1956; Email: donglee@pusan.ac.kr

Authors

Chengguo Li − *School of Mechanical Engineering, Pusan National University, Busan 609-735, South Korea*

Hakgyu Yi − *School of Mechanical Engineering, Pusan National University, Busan 609-735, South Korea*

Seongyong Eom − *School of Mechanical Engineering, Pusan National University, Busan 609-735, South Korea*

Gyungmin Choi − *School of Mechanical Engineering, Pusan National University, Busan 609-735, South Korea*

Tae-Youl Choi − *Department of Mechanical and Energy Engineering, University of North Texas, Denton, Texas 76207, United States*

Complete contact information is available at: https://pubs.acs.org/10.1021/acs.energyfuels.9b04387

Notes

The authors declare no competing financial interest.

■ ACKNOWLEDGMENTS

This work was supported by a 2-Year Research Grant of Pusan National University.

■ REFERENCES

(1) Giddey, S.; Badwal, S. P. S.; Kulkarni, A.; Munnings, C. A comprehensive review of direct carbon fuel cell technology. *Prog. Energy Combust. Sci.* **2012**, *38*, 360−399.

(2) Cao, D.; Sun, Y.; Wang, G. Direct carbon fuel cell: Fundamentals and recent developments. *J. Power Sources* **2007**, *167*, 250−257.

(3) Elleuch, A.; Boussetta, A.; Halouani, K. Analytical modeling of electrochemical mechanisms in CO_2 and CO/CO_2 producing direct carbon fuel cell. *J. Electroanal. Chem.* **2012**, *668*, 99−106.

(4) Vutetakis, D. G.; Skidmore, D. R.; Byker, H. J. Electrochemical oxidation of molten carbonate−coal slurries. *J. Electrochem. Soc.* **1987**, *134*, 3027−3035.

(5) Dudek, M.; Tomczyk, P.; Socha, R.; Hamaguchi, M. Use of ash-free "Hyper-coal" as a fuel for a direct carbon fuel cell with solid oxide electrolyte. *Int. J. Hydrogen Energy* **2014**, *39*, 12386−12394.

(6) Lee, C. G.; Kim, W. K. Oxidation of ash-free coal in a direct carbon fuel cell. *Int. J. Hydrogen Energy* **2015**, *40*, 5475−5481.

(7) Kaklidis, N.; Garagounis, I.; Kyriakou, V.; Besikiotis, V.; Arenillas, A.; Menendez, J. A.; Marnellos, G. E.; Konsolakis, M. Direct utilization of lignite coal in a Co-CeO_2/YSZ/Ag solid oxide fuel cell. *Int. J. Hydrogen Energy* **2015**, *40*, 14353−14363.

(8) Li, X.; Zhu, Z.; Marco, R. D.; Dicks, A.; Bradley, J.; Liu, S.; Lu, G. Q. Factors that determine the performance of carbon fuels in the direct carbon fuel cell. *Ind. Eng. Chem. Res.* **2008**, *47*, 9670−9677.

(9) Li, X.; Zhu, Z.; De Marco, R.; Bradley, J.; Dicks, A. Carbon nanofibers synthesized by catalytic decomposition of methane and their electrochemical performance in a direct carbon fuel cell. *Energy Fuels* **2009**, *23*, 3721−3731.

(10) Jiang, C.; Ma, J.; Corre, G.; Jain, S. L.; Irvine, J. T. S. Challenges in developing direct carbon fuel cells. *Chem. Soc. Rev.* **2017**, *46*, 2889−2912.

(11) Jiang, C.; Ma, J.; Bonaccorso, A. D.; Irvine, J. T. S. Demonstration of high power, direct conversion of waste-derived carbon in a hybrid direct carbon fuel cell. *Energy Environ. Sci.* **2012**, *5*, 6973−6980.

(12) Li, C.; Lee, E. K.; Kim, Y. T.; Lee, D. Enhancing triple-phase boundary at fuel electrode of direct carbon fuel cell using a fuel-filled ceria coated porous anode. *Int. J. Hydrogen Energy* **2014**, *39*, 17314−17321.

(13) Li, C.; Yi, H.; Jalalabadi, T.; Lee, D. Thermal decomposition of alkane hydrocarbons inside a porous Ni anode for fuel supply of direct carbon fuel cell: Effects of morphology and crystallinity of carbon. *J. Power Sources* **2015**, *294*, 284−291.

(14) Li, C.; Yi, H.; Lee, D. On-demand supply of slurry fuels to a porous anode of direct carbon fuel cell: Attempts to increase fuel-anode contact and realize long-term operation. *J. Power Sources* **2016**, *309*, 99−107.

(15) Li, X.; Zhu, Z.; De Marco, R.; Bradley, J.; Dicks, A. Evaluation of raw coals as fuels for direct carbon fuel cells. *J. Power Sources* **2010**, *195*, 4051−4058.

(16) Ahn, S. Y.; Eom, S. Y.; Rhie, Y. H.; Sung, Y. M.; Moon, C. E.; Choi, G. M.; Kim, D. J. Application of refuse fuels in a direct carbon fuel cell system. *Energy* **2013**, *51*, 447−456.

(17) Ahn, S. Y.; Eom, S. Y.; Rhie, Y. H.; Sung, Y. M.; Moon, C. E.; Choi, G. M.; Kim, D. J. Utilization of wood biomass char in a direct carbon fuel cell (DCFC) system. *Appl. Energy* **2013**, *105*, 207−216.
(18) Eom, S. Y.; Ahn, S. Y.; Rhie, Y. H.; Kang, K. J.; Sung, Y. M.; Moon, C. E.; Choi, G. M.; Kim, D. J. Influence of devolatilized gases composition from raw coal fuel in the lab scale DCFC (direct carbon fuel cell) system. *Energy* **2014**, *74*, 734−740.
(19) Eom, S. Y.; Cho, J. M.; Ahn, S. Y.; Sung, Y. M.; Choi, G. M.; Kim, D. J. Comparison of the electrochemical reaction parameter of graphite and sub-bituminous coal in a direct carbon fuel cell. *Energy Fuels* **2016**, *30*, 3502−3508.
(20) Jalalabadi, T.; Li, C.; Yi, H.; Lee, D. A TGA study of CO_2 gasification reaction of various types of coal and biomass. *J. Mech Sci. Technol.* **2016**, *30*, 3275−3281.
(21) Tang, Y.; Liu, J. Effect of anode and boudouard reaction catalyst on the performance of direct carbon solid oxide fuel cells. *Int. J. Hydrogen Energy* **2010**, *35*, 11188−11193.
(22) Liu, J.; Ye, K.; Cheng, K.; Wang, G.; Yin, J.; Cao, D. The catalytic effect of CeO_2 for electrochemical oxidation of graphite in molten carbonate. *Electrochim. Acta* **2014**, *135*, 270−275.
(23) Xu, X.; Zhou, W.; Liang, F.; Zhu, Z. Optimization of a direct carbon fuel cell for operation below 700 °C. *Int. J. Hydrogen Energy* **2013**, *38*, 5367−5374.
(24) Elleuch, A.; Yu, J.; Boussetta, A.; Halouani, K.; Li, Y. Electrochemical oxidation of graphite in an intermediate temperature direct carbon fuel cell based on two-phases electrolyte. *Int. J. Hydrogen Energy* **2013**, *38*, 8514−8523.
(25) Kim, Y.; Kim, Y. T.; Kim, S.; Lee, D. Catalytic oxidation kinetics of iron-containing carbon particles generated by spraying ferrocene-mixed diesel fuel into hydrogen-air diffusion flame. *Carbon* **2010**, *48*, 2072−2084.
(26) Wang, L.; Song, C.; Song, J.; Lv, G.; Pang, H.; Zhang, W. Aliphatic C-H and oxygenated surface functional groups of diesel in-cylinder soot: Characterizations and impact on soot oxidation behavior. *Proc. Combust. Inst.* **2013**, *34*, 3099−3106.
(27) Castellano, M.; Turturro, A.; Riani, P.; Montanari, T.; Finocchio, E.; Ramis, G.; Busca, G. Bulk and surface properties of commercial kaolins. *Appl. Clay Sci.* **2010**, *48*, 446−454.
(28) Tulloch, J.; Allen, J.; Wibberley, L.; Donne, S. Influence of selected coal contaminants on graphitic carbon electro-oxidation for application to the direct carbon fuel cell. *J. Power Sources* **2014**, *260*, 140−149.
(29) Siengchum, T.; Guzman, F.; Chuang, S. Analysis of gas products from direct utilization of carbon in a solid oxide fuel cell. *J. Power Sources* **2012**, *213*, 375−381.
(30) Park, S.; Vohs, J. M.; Gorte, R. J. Direct oxidation of hydrocarbons in a solid-oxide fuel cell. *Nature* **2000**, *404*, 265−267.
(31) Aliotta, C.; Liotta, L.F.; Deganello, F.; La Parola, V.; Martorana, A. Direct methane oxidation on $La_{1-x}Sr_xCr_{1-y}Fe_yO_{3-\delta}$ perovskite-type oxides as potential anode for intermediate temperature solid oxide fuel cells. *Appl. Catal., B* **2016**, *180*, 424−433.
(32) Lee, C. G.; Hur, H.; Song, M. B. Oxidation behavior of carbon in a coin-type direct carbon fuel cell. *J. Electrochem. Soc.* **2011**, *158*, B410−B415.
(33) Lahijani, P.; Zainal, Z.; Mohammadi, M.; Mohamed, A. Conversion of the greenhouse gas CO_2 to the fuel gas CO via the Boudouard reaction: A review. *Renewable Sustainable Energy Rev.* **2015**, *41*, 615−632.
(34) Zhang, L.; Huang, J.; Fang, Y.; Wang, Y. Gasification Reactivity and Kinetics of Typical Chinese Anthracite Chars with Steam and CO_2. *Energy Fuels* **2006**, *20*, 1201−1210.
(35) Sakawa, M.; Sakurai, Y.; Hara, Y. Influence of coal characteristics on CO_2 gasification. *Fuel* **1982**, *61*, 717−720.
(36) Ravi, S.; Dharmarajan, R.; Moghaddam, S. Measurement of capillary radius and contact angle within porous media. *Langmuir* **2015**, *31*, 12954−12959.
(37) Ahmed, T.; Semmens, M. J.; Voss, M. A. Oxygen transfer characteristics of hollow fiber, composite membranes. *Adv. Environ. Res.* **2004**, *8*, 637−646.
(38) Washburn, E. W. The dynamics of capillary flow. *Phys. Rev.* **1921**, *17*, 273−283.
(39) Chen, C.; Maruyama, T.; Hsieh, P.; Selman, J. Wetting behavior of carbon in molten carbonate. *J. Electrochem. Soc.* **2012**, *159*, D597−D604.
(40) Cherepy, N. J.; Krueger, R.; Fiet, K. J.; Jankowski, A. F.; Cooper, J. F. Direct conversion of carbon fuels in a molten carbonate fuel cell. *J. Electrochem. Soc.* **2005**, *152*, A80.
(41) Eom, S. Y.; Ahn, S. Y.; Rhie, Y. H.; Choi, G. M.; Kim, D. J. Effect of coal gases on electrochemical reactions in the direct carbon fuel cell system. *J. Clean Energy Technol.* **2015**, *3*, 72−77.
(42) Cao, D.; Wang, G.; Wang, C.; Wang, J.; Lu, T. Enhancement of electrooxidation of activated carbon for direct carbon fuel cell. *Int. J. Hydrogen Energy* **2010**, *35*, 1778−1782.

https://dx.doi.org/10.1021/acs.energyfuels.9b04387
Energy Fuels 2020, 34, 4129−4138